Applied Radiation and Isotopes 201 (2023) 110997

Contents lists available at ScienceDirect

Applied Radiation and Isotopes

journal homepage: www.elsevier.com/locate/apradiso

Luminescence characterization of BioGlass undoped and doped with europium and silver ions

Anderson M.B. Silva [a,*], Laís S. Jesus [b], Wender Correa [b], Danilo O. Junot [c], Linda V.E. Caldas [d], Noelio O. Dantas [b], Divanizia N. Souza [a], Anielle C.A. Silva [b]

[a] Departamento de Física, Universidade Federal de Sergipe, Marechal Rondon, S/N, 49.100-000, São Cristovão, SE, Brazil
[b] Laboratório de Novos Materiais Nanoestruturados e Funcionais, Instituto de Física, Universidade Federal de Alagoas, 57072-900, Maceió, Alagoas, Brazil
[c] Instituto de Física Armando Dias Tavares, Universidade do Estado do Rio de Janeiro UERJ, Rua São Francisco Xavier, 524, 20550-013, Rio de Janeiro, RJ, Brazil
[d] Instituto de Pesquisas Energéticas e Nucleares, Comissão Nacional de Energia Nuclear, IPEN/CNEN-SP, Av. Prof. Lineu Prestes, 2242, 05508-000, São Paulo, SP, Brazil

ARTICLE INFO

Keywords:
BioGlass
Ag nanoparticles
Europium ions
Structural properties
Optical properties
Thermoluminescence
Optically stimulated luminescence

ABSTRACT

The objective of this study was to investigate the properties of BioGlass, with and without doping with europium and silver, with a specific focus on its potential application in thermoluminescent (TL) and optically stimulated luminescent (OSL) dosimetry. The structural and optical characteristics of the samples were also analyzed using techniques such as X-ray diffraction (XRD), optical absorption (OA), and fluorescence spectroscopy (FL). An XRD analysis confirmed the amorphous phase of the BioGlass. OA and FL spectra were obtained at room temperature, and characteristic bands of dopant ions were observed which confirmed the incorporation of the Eu^{3+} ions and silver nanoparticles Ag(NP) ion into the BioGlass. The OSL decay curves exhibited a characteristic exponential behavior, with a notable presence of fast and medium decay components; this suggests that the charge traps within the BioGlass samples possess a high photoionization cross section when exposed to blue LEDs, which are commonly used as the light source in OSL readers. Different TL glow peaks with varying shapes of the glow curve were observed when the dopant, the co-dopant, and the concentration of silver were altered in the samples. The TL kinetic parameters were determined, such as the order value, activation energy, and frequency factor, and the OSL parameters for the compound were also analyzed, including an exponential fit to the curves. Based on these initial results, we conclude that BioGlass has the potential for use in radiation dosimetry.

1. Introduction

In recent decades, significant attention has been paid to the use of synthetic inorganic amorphous biomaterials, and particularly BioGlasses, due to their extensive range of applications in various technological fields. These materials have found uses in osteoconductive applications, including restorative materials, bone grafts, implant coatings, and tissue engineering scaffolds (Farooq et al., 2019). Moreover, in some groups of BioGlasses, silver doping can be used to enhance the antibacterial effects (Kwakye-Awuah et al., 2008). The different types of BioGlass proposed in the literature have been critically examined, discussed, and compared, and for a more comprehensive review, the reader is referred to (Baino and Vitale-Brovarone, 2011).

Scientific investigation of rare earth (RE) activated luminescence materials has intensified recently, largely due to their excellent luminescent properties, which enable the application of these materials in many technological fields such as conversion materials for solar cells, fiber amplifiers, solid-state lasers, radiation detectors, photoelectric devices, and optical data storage. Of the numerous RE ions, Eu and Tb ions are often chosen for incorporation into materials of interest for luminescent dosimetry, as they give characteristic emission lines when excited with ionizing radiation (Ziya Halefoglu et al., 2019; Halefoglu et al., 2020; Portakal Ucar et al., 2020; Sarikci et al., 2023; Silva et al., 2021, 2022). The incorporation of silver as a co-dopant has also attracted considerable attention, as this metal improves the luminescent properties of $CaSO_4$:Eu and $CaSO_4$:Tb (Silva et al., 2020; Junot et al., 2014, 2019). Silver is able to generate structure defects more satisfactorily when incorporated as co-dopant, possibly through acting as an energy transfer ion (Silva et al., 2021).

The use of BioGlass in the body, especially in hard tissues, requires a

* Corresponding author.
E-mail address: andersonmanoel22@hotmail.com (A.M.B. Silva).

https://doi.org/10.1016/j.apradiso.2023.110997
Received 16 May 2023; Received in revised form 27 July 2023; Accepted 22 August 2023
Available online 23 August 2023

significant degree of care when undertaking radiological procedures. The effects of radiation and its interaction with tissue directly impact the body's tissues during both treatment and diagnostic procedures, and this has raised concerns regarding potential clinical outcomes (Tekin et al., 2021). Recent studies also have proposed the application of thermoluminescent (TL) and optically stimulated luminescent (OSL) dosimetry as alternative experimental techniques to evaluate the different responses of BioGlass to ionizing radiation (Polymeris et al., 2011, 2017; Kumar et al., 2021). These techniques involve acquiring emission signals from BioGlass samples, and can provide valuable information about the dose of radiation absorbed by the material.

When exposed to ionizing radiation, the energy absorbed by a luminescent material causes trapping of electrons or holes in the bandgap between the valence band and the conduction band. In the case of crystalline materials, crystal lattice defects facilitate the trapping of free electrons and holes in metastable states. During the luminescent reading process, an external stimulus such as heat (TL) or light (OSL) is applied to the material, thereby promoting the detrapping and recombination of electrons and holes. This recombination process leads to the emission of light, which is known as luminescence. The thermal or optical luminescence of amorphous materials such as glasses can also be interpreted based on this bandgap model (Polymeris et al., 2017; Bradley et al., 2020).

The amount of light emitted during heating of the material can be measured, and is directly related to the number of trapped electric charges, which depends on the exposure of the material to radiation. It then becomes possible to establish a correlation between the absorbed dose and the intensity of the TL/OSL signal exhibited by the material (Halefoglu et al., 2020). Through the use of TL and OSL techniques, we aim to assess the potential of modified biomaterials for radiation dosimetry applications. We believe that by addressing this research gap, our study can contribute to the development of new biomaterials that are suitable for dosimetric applications.

In this work, we investigated the optical, structural and dosimetric properties of a BioGlass, with and without doping with europium ions and silver nanoparticles. TL and OSL techniques were applied to assess the potential of the new materials for use in radiation dosimetry. Since no existing work could be found on the use of BioGlass doped with europium and silver nanoparticles in radiation dosimetry using the TL or OSL techniques, we aimed to evaluate these approaches and to develop a new biomaterial that was suitable for dosimetric applications.

2. Materials and methods

Samples of BioGlass undoped and doped with 2 wt% of europium (Eu) and co-doped with 0.50 and 0.25 of silver (Ag) ions were synthesized using a patented methodology (no. BR1020230000622). The structural properties of the samples were analyzed using X-ray diffraction (XRD) with a Shimadzu XRD 6000 instrument, employing Cu-Kα radiation (λ = 1.5406 Å). XRD patterns were produced over the range 10°–100° (2θ), with a step size of 0.02°. Optical absorption (OA) spectra were recorded using a Shimadzu UV-VIS-NIR -3600 spectrometer with resolution ±1 nm. The fluorescence (FL) spectra were recorded using a Spex Fluorolog-3 Spectrofluorometer (Jobin Yvon Inc., Edison, NJ, USA) with a 450 W Xe light source. All of the characterizations were performed at room temperature.

For the TL and OSL measurements, samples were produced in powder form, and were weighed and pressed using a stainless steel die. A compressive force of ~100 kgf was applied for a period of 10 s to produce pellets 6 mm in diameter and 1 mm in thickness, with an approximate weight of 30 mg. After the pressing process, the pellets were sintered at 600 °C for 1 h. The TL/OSL signals of the samples were measured using a Risø TL/OSL DA-20 automatic reader. To ensure accurate measurements, background subtraction was performed to eliminate any undesired signals that were unrelated to the luminescent response of the samples to the radiation dose.

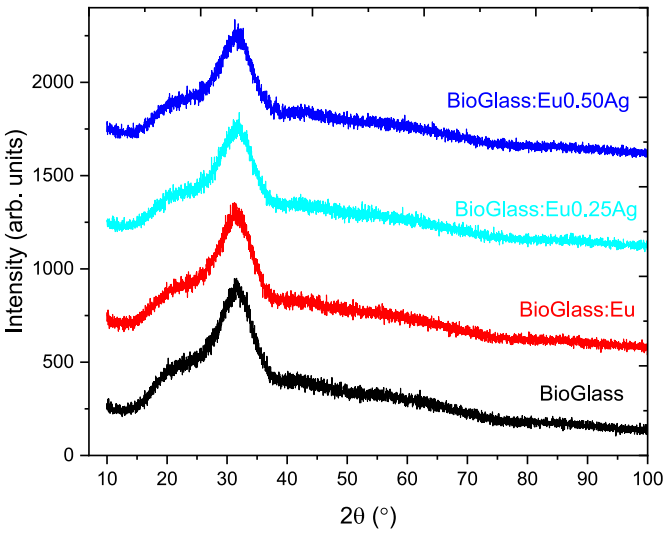

Fig. 1. X-ray diffraction results for BioGlass, with and without doping with europium and silver (0.25 and 0.50) ions.

BioGlass pellets were irradiated using a beta source, which was connected to the Risø system at a dose rate of 81.6 mGy/s. During the TL/OSL measurements, a Hoya U-340 filter with a wavelength range of (340 ± 40) nm was used in the reader. To obtain the OSL readings, samples were exposed to blue LEDs emitting light at a wavelength of 470 nm. All measurements were conducted in continuous wave mode. The experimental OSL decay curves were characterized by three exponential decay functions, which were derived by fitting the data using Equation (1):

$$I_{OSL} = A_1 e^{-t/\tau_1} + A_2 e^{-t/\tau_2} + A_3 e^{-t/\tau_3} \quad (1)$$

where I_{OSL} is the total OSL intensity; A_1, A_2, and A_3 are constant coefficients related to the decay components: fast (A_1), medium (A_2), and slow (A_3); and τ_1, τ_2, and τ_3 are decay constants which reflect the probability of trapped electrons escaping to the conduction band over time, under optical stimulation, in different trap sets (Barve et al., 2015; Valença et al., 2018).

The TL glow curves for the samples were recorded at a heating rate of 10 °C/s. Deconvolution of the glow curves and determination of TL kinetic parameters were performed using OriginLab 8.0 software

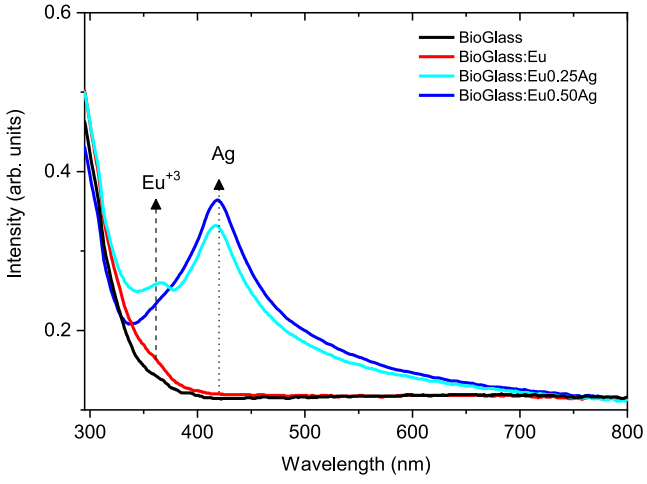

Fig. 2. Optical absorption spectra for BioGlass, with and without doping with europium and silver (0.25 and 0.50) ions.

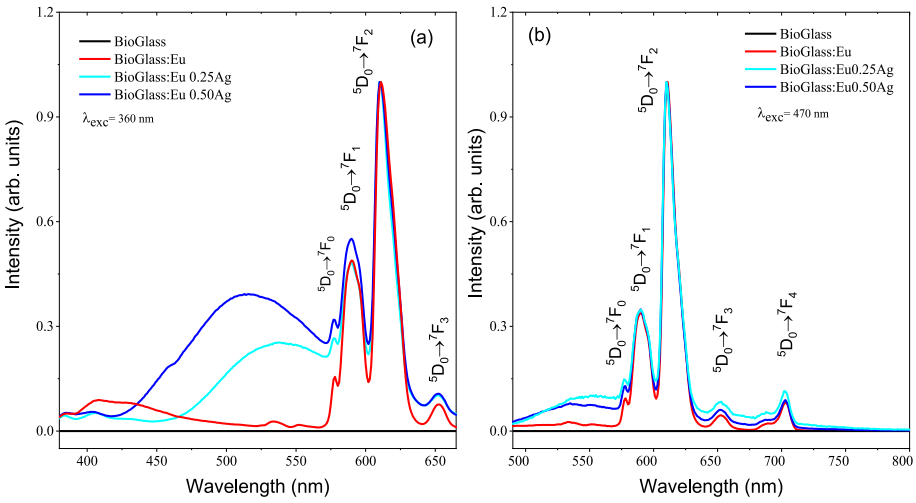

Fig. 3. Fluorescence emission spectra for BioGlass, with and without doping with europium and silver (0.25 and 0.50) ions, under excitation at (a) 360 nm and (b) 470 nm.

(OriginLab Co., USA). The TL curve was analyzed by fitting using the equation proposed by Chen and McKeever (1997) for the general kinetic order, which allowed us to determine the kinetic order (b), activation energy (E), and frequency factor (s) parameters of the TL peaks. Following each TL/OSL measurement, the pellets underwent annealing at 400 °C for 1 h in a programmable oven before being reused.

3. Results and discussion

3.1. Structural properties

The XRD patterns for the BioGlass with and without doping with europium and silver (0.25 and 0.50) ions are shown in Fig. 1. The diffractograms showed a broad diffraction band characteristic of amorphous samples, and no evidence of secondary phases or impurities was detected, indicating that the Eu^{3+} and Ag ions were completely dissolved in the BioGlass without inducing significant changes.

3.2. Optical absorption and fluorescence spectroscopy studies

Fig. 2 shows the UV–Vis–NIR OA spectra for undoped BioGlass and BioGlass doped with europium and silver (0.25 and 0.50) ions, which were recorded at room temperature over the wavelength range 300–800 nm. For all samples, the OA spectra showed an absorption band below 400 nm, which is characteristic of insulating materials (in this case BioGlass). In the doped samples, however, a redshift was observed due to the absorption of europium ions ($^7F_0 \rightarrow {}^5D_4$ transitions) (Shwetha and Eraiah, 2018) and in those co-doped with silver, a plasmonic band was observed around 419 nm, which is characteristic of silver nanoparticles.

Complementary information was provided by a fluorescence emission study of the samples. Fig. 3 presents the emission spectra for the BioGlass with and without doping, excited at 360 and 470 nm. The characteristic transitions of Eu^{3+} ions in the range 570–720 nm were assigned for all bands. The five peaks in Fig. 3(b) can be attributed to the $^5D_0 \rightarrow {}^7F_0$, $5D_0 \rightarrow {}^7F_1$, $^5D_0 \rightarrow {}^7F_2$,$^5D_0 \rightarrow {}^7F_3$ and $^5D_0 \rightarrow {}^7F_4$ transitions (Nardi et al., 2015; Yang et al., 2012).

The less intense peaks at ~385, 410, 536 and 550 nm are ascribed to the intra-configurational 4f-4f transitions of the Eu^{3+} ions in this host lattice. The four peaks in Fig. 3(a) can be related to the $^7F_0 \rightarrow {}^5L_6$, $^7F_0 \rightarrow {}^5D_3$, $^7F_0 \rightarrow {}^5D_1$ and $^7F_2 \rightarrow {}^5D_1$ transitions (Yang et al., 2012; Carnall et al., 1989). Furthermore, the samples co-doped with silver showed fluorescence spectra that were significantly modified in the range 420–570 nm. The broad band observed in Ag-doped samples near 500 nm is due to the surface plasmon resonance in the Ag nanoparticles

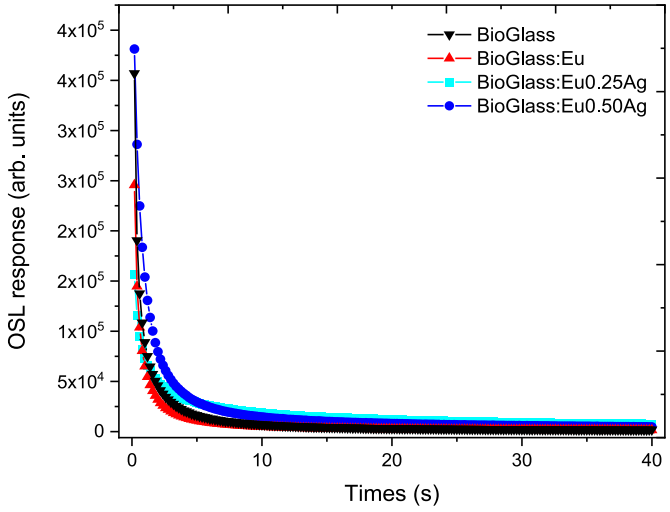

Fig. 4. Typical OSL emission from undoped and doped BioGlass irradiated with 10 Gy ($^{90}Sr+{}^{90}Y$).

incorporated into the BioGlass (Le et al., 2022). The incorporation of silver dopants into the BioGlass material leads to an improvement in the material's fluorescence behavior, particularly in this range of wavelengths. These results suggest that the introduction of silver nanoparticles affects the emission properties of the material, potentially resulting in an improvement in luminescence.

The composition and phase of the doped and undoped BioGlass obtained from the XRD analysis show that there is no apparent difference after doping with Eu^{3+} or the addition of Ag nanoparticles, despite confirmation of the incorporation of europium and silver into the matrix via optical characterization.

3.3. OSL results

The typical exponential decay curves in Fig. 4 represent the OSL signals from the BioGlass, with and without doping with europium and silver (0.25 and 0.50) ions, after 10 Gy of beta irradiation. In this analysis, the samples were stimulated with blue light for a duration of 40 s. As the traps are emptied, the OSL signal exhibits an exponential decrease. This suggests that the OSL response of these samples is highly susceptible to stimulation at 470 nm, indicating that the traps have a high photoionization cross section for blue LEDs. Consequently, these

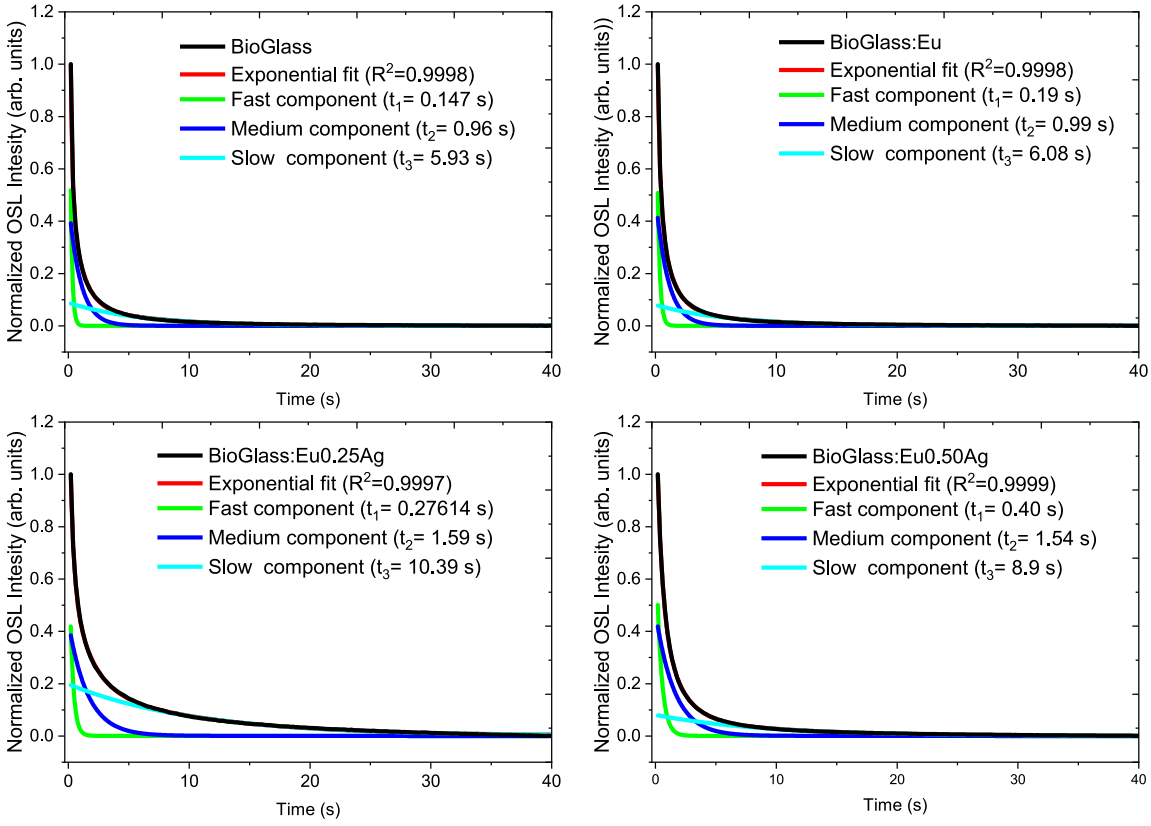

Fig. 5. Experimental and fitted OSL decay curves for undoped BioGlass, BioGlass:Eu, BioGlass:Eu0.25Ag and BioGlass:Eu0.50Ag samples.

Table 1
OSL parameters obtained from an exponential fit of the curves for the compound.

Type of sample	CW-OSL component	Coefficient A_i	Decay constant t_i (s)	Exponential fit
BioGlass	**Fast**	2.021 ± 0.031 (A_1)	0.147 ± 0.002 (t_1)	R^2: 0.9998
	Medium	0.482 ± 0.007 (A_2)	0.964 ± 0.017 (t_2)	
	Slow	0.08 ± 0.002 (A_3)	5.932 ± 0.089 (t_3)	
BioGlass:Eu	**Fast**	1.442 ± 0.012 (A_1)	0.191 ± 0.003 (t_1)	R^2: 0.9998
	Medium	0.5045 ± 0.008 (A_2)	0.999 ± 0.011 (t_2)	
	Slow	0.079 ± 0.002 (A_3)	6.087 ± 0.118 (t_3)	
BioGlass: Eu0.25Ag	**Fast**	0.8642 ± 0.008 (A_1)	0.276 ± 0.005 (t_1)	R^2: 0.9997
	Medium	0.435 ± 0.006 (A_2)	1.591 ± 0.029(t_2)	
	Slow	0.198 ± 0.002 (A_3)	10.394 ± 0.085 (t_3)	
BioGlass: Eu0.50Ag	**Fast**	0.816 ± 0.006 (A_1)	0.409 ± 0.042(t_1)	R^2: 0.9999
	Medium	0.476 ± 0.007 (A_2)	1.546 ± 0.018 (t_2)	
	Slow	0.080 ± 0.001 (A_3)	8.939 ± 0.1027 (t_3)	

findings indicate significant potential for the use of these samples in OSL dosimetry applications.

The incorporation of europium into the BioGlass resulted in a reduction of the OSL intensity of the samples; in contrast, there was a noticeable increase in the intensity of the OSL response of the samples co-doped with silver at a concentration of 0.50 mol%.

Co-doping has been shown to be effective in resolving the charge imbalance caused by the incorporation of europium into BioGlass structures. Previous studies have demonstrated that co-doping with alkali metal ions and transition metals can significantly improve the luminescence efficiency of these materials, possibly by acting as charge compensators and facilitating the incorporation of lanthanide dopants into their structures (Yukihara et al., 2014; Altunal et al., 2021; Dorenbos, 2017).

The OSL decay curves for the samples were well fitted by a triple exponential decay, as described in Equation (1). The exponential fitting of the OSL decay curves in Fig. 5 gave constant coefficients and decay constants, which are presented in Table 1. The samples had higher values for A_1 and A_2 than for A_3, thus confirming the predominance of OSL decay curves with fast and medium components. The highest values of A_1 and A_2 were seen for undoped BioGlass, followed by the BioGlass:Eu, BioGlass:Eu0.25Ag and BioGlass:Eu0.50Ag samples, respectively. The significance of the slow component was minimal, since the highest value of A_3 was only 0.107 for the OSL response of the samples analyzed here. The decay constants (lifetimes) of the components for each sample are also shown in Table 1.

The curve-fitting equation with three components was applied based on its ability to provide an accurate description of the decay model, as evidenced by an adjusted R-squared value of higher than 0.9975. In comparison, the decay model with two components was considered an imprecise estimate. It is important to note that the curve-fitting approach based on three exponential decays is an approximation, and represents mathematical consistency rather than definitive evidence of distinct physical mechanisms (Altunal et al., 2018). To gain a deeper understanding of the traps and transitions involved in OSL development, further studies focusing on the numerical solutions of the charge

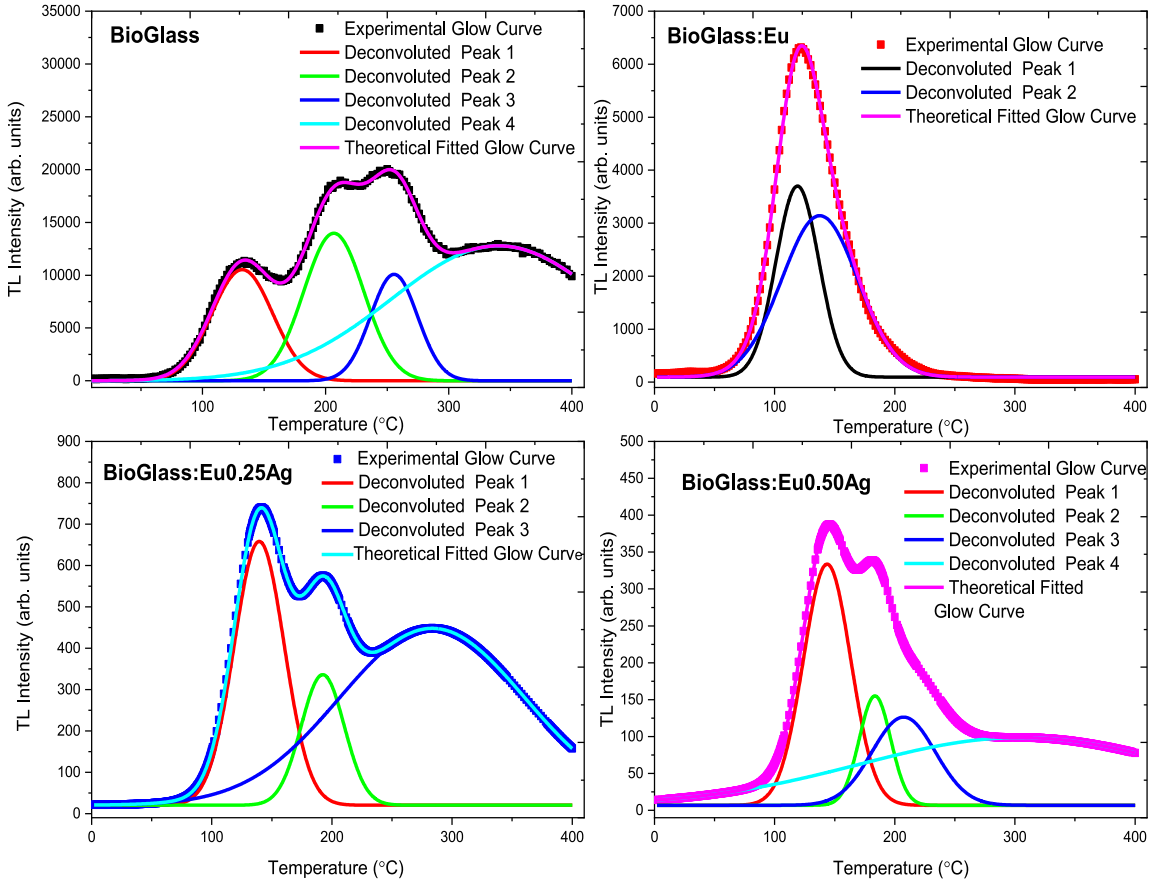

Fig. 6. TL glow curve deconvolution for samples of undoped BioGlass, BioGlass:Eu, BioGlass:Eu0.25Ag and BioGlass:Eu0.50Ag.

Table 2
Parameters of the TL glow curves for undoped BioGlass, BioGlass:Eu, BioGlass:Eu0.25Ag and BioGlass:Eu0.50Ag samples (determined using the general kinetic order equation described by Chen and McKeever (1997)).

Type of sample		T_m (K)	I_m (arb. units)	b (kinetic order)	E (eV)	S (s^{-1})
BioGlass	Peak 1	405.99 ± 0.51	10663.28 ± 11.92	1.59 ± 0.01	0.74 ± 0.01	2.3×10^{10}
	Peak 2	479.81 ± 0.62	14207.32 ± 18.88	1.68 ± 0.02	1.09 ± 0.01	4.0×10^{12}
	Peak 3	528.77 ± 0.26	10207.11 ± 14.31	1.70 ± 0.01	1.75 ± 0.01	9.3×10^{17}
	Peak 4	602.74 ± 0.09	12697.26 ± 16.19	1.46 ± 0.01	0.38 ± 0.01	4.5×10^{3}
BioGlass:Eu	Peak 1	392.18 ± 0.23	3744.16 ± 10.11	1.69 ± 0.01	0.96 ± 0.01	4.1×10^{13}
	Peak 2	409.97 ± 0.19	3165.00 ± 6.06	1.47 ± 0.01	0.52 ± 0.02	2.3×10^{7}
BioGlass:Eu0.25Ag	Peak 1	412.48 ± 0.11	664.30 ± 1.98	1.68 ± 0.02	0.89 ± 0.01	1.2×10^{12}
	Peak 2	465.07 ± 0.08	336.19 ± 1.94	1.84 ± 0.04	1.34 ± 0.02	6.3×10^{15}
	Peak 3	479.81 ± 0.53	442.88 ± 0.51	1.11 ± 0.01	0.31 ± 0.01	7.6×10^{3}
BioGlass:Eu0.50Ag	Peak 1	416.94 ± 0.17	337.49 ± 0.66	1.66 ± 0.01	0.98 ± 0.01	1.2×10^{13}
	Peak 2	456.54 ± 0.13	155.84 ± 0.78	1.84 ± 0.04	1.84 ± 0.02	5.6×10^{21}
	Peak 3	492.70 ± 0.19	126.58 ± 0.56	1.76 ± 0.03	0.94 ± 0.01	4.8×10^{10}
	Peak 4	595.54 ± 0.41	98.82 ± 0.15	1.94 ± 0.06	0.19 ± 0.05	4.6×10^{3}

trafficking equations are required (Altunal et al., 2022). However, the values of the parameters associated with OSL emission, which is characterized by an initial fast decay followed by a slower decay, provide evidence for the involvement of trapping centers with varying photoionization cross-sections (Daniel et al., 2016).

3.4. TL results

In this section, the TL glow curves for the BioGlasses produced are analyzed. The samples were previously irradiated with an absorbed dose of 10 Gy of beta radiation. Fig. 6 shows the TL glow curves obtained for undoped BioGlass, BioGlass:Eu, BioGlass:Eu0.25Ag and BioGlass:Eu0.50Ag samples after irradiation. The TL from undoped bioglass shows three peaks at approximately 132 °C, 206 °C and 255 °C, and a peak shoulder can also be observed at approximately 300 °C.

The TL glow curves for the Eu-doped samples show a main peak at approximately 125 °C, which results from the overlapping of two intense peaks at around 119 °C and 137 °C. The samples co-doped with silver contain more peaks than the europium-doped samples. The Ag co-doping of the BioGlass:Eu glass-ceramic changes in the TL emission can be associated with the addition of recombination centers located at deeper levels, as similar behavior was reported by Silva et al. (2020) for $CaSO_4$ samples doped with silver in the form of silver oxide (Ag_2O) and silver nanoparticle (Ag(NP)).

The addition of silver as a co-dopant in the BioGlass:Eu matrix induces a shift in the TL peaks at 200 °C and 300 °C to higher

temperatures, which may lead to a greater interest in the use of BioGlass: Eu, Ag in TL dosimetry.

Table 2 shows the TL parameters for the bioglass obtained from a general kinetic order fitting, as described by Chen and McKeever (1997). The peak temperatures (Tm), maximum peak intensities (Im), kinetic order values (b), activation energies (E), and frequency factors (s) were determined using OriginLab 8.0 software. In numerous TL applications, a clear knowledge of these physical parameters is crucial (Tamrakar et al., 2015).

From Table 2, we can observe a temperature variation in the first peak between 392 and 416 K. The trapping centers are located between 1.59 and 1.69 eV for the group of samples evaluated here. The second TL peaks for the undoped BioGlass, BioGlass:Eu, BioGlass:Eu0.25Ag and BioGlass:Eu0.50Ag samples are located at 479.81 ± 0.62, 409.97 ± 0.19, 465.07 ± 0.08 and 456.54 ± 0.13 K, respectively. Trapping centers located between 0.52 and 1.84 eV were revealed. The third TL peaks for the bioglass samples are located at temperatures of 528.77 ± 0.26, 479.81 ± 0.53 and 492.70 ± 0.19 K, respectively, and the trapping centers are located between 0.31 and 1.75 eV.

The fourth TL peaks for the BioGlass and BioGlass:Eu0.50Ag samples showed very broad bands, suggesting the presence of trapping centers with low activation energies (0.19 and 0.38 eV). The incorporation of silver as a co-dopant in the BioGlass:Eu matrix introduced at least three overlapping peaks within the TL glow curve, which suggests the formation of a continuum of closely located energy states.

All the deconvolved TL peaks presented kinetic orders of between one and two, indicating the existence of a general kinetic order in the TL process. The frequency factors for the trap centers involved in the TL emission were also determined.

The BioGlass:Eu0.25Ag and BioGlass:Eu0.50Ag samples showed TL intensities on the same order of magnitude, but the TL sensitivity of the BioGlass samples was nine times higher than that of the BioGlass:Eu samples, and 30 times higher than the TL sensitivity of the samples co-doped with silver nanoparticles.

4. Conclusion

Although there is an extensive body of literature on the various properties of several types of BioGlasses, recent studies have proposed the use of TL and OSL dosimetry as alternative experimental techniques for determining the effective differences between the responses of BioGlasses. In this study, the specific luminescence of undoped and doped BioGlass was analyzed using the TL and OSL techniques, and structural and optical characterizations were carried out. An XRD analysis confirmed the amorphous nature of both undoped and doped BioGlass, and the OA and fluorescence results confirmed the presence of Eu^{3+} and Ag ions in the BioGlass. The samples showed a typical OSL exponential signal decay, with a predominance of fast and medium components, implying that the charge traps have a high photoionization cross section for blue LEDs. A determination of the trap depth parameters (Tm, Im, b, E and s) for the TL glow peaks of the different samples provided the missing data needed to understand the energies associated with the capture centers formed in the glass that give rise to the TL signal. For silver co-doped BioGlass, the charge traps are located deeper, with higher activation energies and peak temperatures, which could (at least in theory) reduce the peak signal fading over time. These materials have characteristics that suggest potential for use in TL and OSL dosimeters. A thorough dosimetric characterization is currently under way, and will be published in the near future. Based on these initial results, we conclude that BioGlass shows potential for use in radiation dosimetry.

CRediT authorship contribution statement

Anderson M.B. Silva: Writing – review & editing, Project administration, Methodology, Investigation, Formal analysis, Conceptualization. **Laís S. Jesus:** Methodology, Investigation. **Wender Correa:** Visualization, Investigation. **Danilo O. Junot:** Data curation, Investigation, Writing - review & editing. **Linda V.E. Caldas:** Conceptualization, Visualization, Resources, Supervision. **Noelio O. Dantas:** Visualization, Investigation. **Divanizia N. Souza:** Conceptualization, Project administration, Supervision, Validation, Visualization. **Anielle C.A. Silva:** Conceptualization, Methodology, Visualization, Resources, Supervision.

Declaration of competing interest

The authors declare that they have no known competing financial interests or personal relationships that could have appeared to influence the work reported in this paper.

Data availability

Data will be made available on request.

Acknowledgments

The authors are grateful to the Brazilian agencies Comissão Nacional de Energia Nuclear (CNEN), Coordenação de Aperfeiçoamento de Pessoal de Nível Superior (CAPES), Conselho Nacional de Desenvolvimento Científico e Tecnológico (CNPq) and Fundação de Amparo à Pesquisa do Estado de São Paulo (FAPESP).

References

Altunal, V., Yegingil, Z., Tuken, T., Depci, T., Ozdemir, A., Guckan, V., Nur, N., Kurt, K., Bulur, E., 2018. Optically stimulated luminescence characteristics of BeO nanoparticles synthesized by sol-gel method. Radiat. Meas. 118, 54–66. https://doi.org/10.1016/j.radmeas.2018.08.009.

Altunal, V., Guckan, V., Ozdemir, A., Ekicibil, A., Karadag, F., Yegingil, I., Zydhachevskyy, Y., Yegingil, Z., 2021. A systematic study on luminescence characterization of lanthanide-doped BeO ceramic dosimeters. J. Alloys Compd. 876, 160105 https://doi.org/10.1016/j.jallcom.2021.160105.

Altunal, V., Guckan, V., Ozdemir, A., Zydhachevskyy, Y., Lawrence, Y., Yu, Y., Yegingil, Z., 2022. Three newly developed BeO-based OSL dosimeters. J. Lumin. 241, 118528 https://doi.org/10.1016/j.jlumin.2021.118528.

Baino, F., Vitale-Brovarone, C., 2011. Three-dimensional glass-derived scaffolds for bone tissue engineering: current trends and forecasts for the future. J. Biomed. Mater. Res. A 97, 514–535. https://doi.org/10.1002/jbm.a.33072.

Barve, R.A., Patil, R.R., Moharil, S.V., Bhatt, B.C., Kulkarni, M.S., 2015. Optically stimulated luminescence in Cu^{+} doped lithium orthophosphate. Phys. B Condens. Matter 458, 117–123. https://doi.org/10.1016/j.physb.2014.11.024.

Bradley, D.A., Khandaker, M.U., Alanazi, A.H., 2020. Irradiated glass and thermoluminescence yield: dosimetric utility reviewed. Radiat. Phys. Chem. 170, 108680 https://doi.org/10.1016/j.radphyschem.2020.108680.

Carnall, W.T., Goodman, G.L., Rajnak, K., Rana, R.S., 1989. A systematic analysis of the spectra of the lanthanides doped into single crystal LaF_3. J. Chem. Phys. 90, 3443. https://doi.org/10.1063/1.455853.

Chen, R., McKeever, S.W.S., 1997. Theory of Thermoluminescence and Related Phenomena. World Scientific, New Jersey.

Daniel, D.J., Raja, A., Madhusoodanan, U., Annalakshmi, O., Ramasamy, P., 2016. OSL studies of alkali fluoroperovskite single crystals for radiation dosimetry. Opt. Mater. 58, 497–503. https://doi.org/10.1016/j.optmat.2016.06.019.

Dorenbos, Pieter, 2017. Charge transfer bands in optical materials and related defect level location. Opt. Mater. 69, 8–22. https://doi.org/10.1016/j.optmat.2017.03.061.

Farooq, I., Ali, S., Husain, S., Khan, E., Hill, R.G., 2019. Bioactive glasses—structure and applications. Adv. Dent. Biomater. 453–476. https://doi.org/10.1016/B978-0-08-102476-8.00017-7.

Halefoglu, Y.Z., Oglakci, M., Portakal, Z.G., Akca, S., Souadi, G.O., Canimoglu, A., Topaksu, M., Can, N., 2020. A study on thermoluminescence behaviour of Eu doped LaB_3O_6 irradiated with beta particles. Radiat. Phys. Chem. 168, 108571 https://doi.org/10.1016/j.radphyschem.2019.108571.

Junot, D.O., Santos, M.A.C., Antonio, P.L., Caldas, L.V.E., Souza, D.N., 2014. Feasibility study of $CaSO_4$:Eu, $CaSO_4$:Eu,Ag and $CaSO_4$:Eu,Ag(NP) as thermoluminescent dosimeters. Radiat. Meas. 71, 99–103. https://doi.org/10.1016/j.radmeas.2014.05.022.

Junot, D.O., Santos, A.G., Antonio, P.L., Rezende, M.V., Souza, D.N., Caldas, L.V.E., 2019. Dosimetric and optical properties of $CaSO_4$:Tm and $CaSO_4$:Tm, Ag crystals produced by a slow evaporation route. J. Lumin. 210, 58–65. https://doi.org/10.1016/j.jlumin.2019.02.005.

Kumar, G.A., Rambabu, Y., Guntu, R.K., Sivaram, K., Reddy, M.S., Rao, C.S., Iyengar, N. C.S.N., 2021. ZrxCa30-xP70 thermoluminescent bio glass, structure and elasticity. J. Mech. Behav. Biomed. Mater. 119, 104517 https://doi.org/10.1016/j.jmbbm.2021.104517.

Kwakye-Awuah, B., Williams, C., Kenward, M.A., Radecka, I., 2008. Antimicrobial action and efficiency of silver-loaded zeolite X. J. Appl. Microbiol. 104, 1516–1524. https://doi.org/10.1111/j.1365-2672.2007.03673.x.

Le, T.H., Kim, J.H., Park, S.J., 2022. A Co-doped carbon dot/silver nanoparticle nanocomposite-based fluorescence sensor for metformin hydrochloride detection. Nanomater 12, 1297. https://doi.org/10.3390/nano12081297.

Nardi, R.P.R.D., Braz, C.E., Camargo, A.S., Ribeiro, S.J., Rocha, L.A., Cassanjes, F.C., Poirier, G., 2015. Effect of lead fluoride incorporation on the structure and luminescence properties of tungsten sodium phosphate glasses. Opt. Mater. 49, 249–254. https://doi.org/10.1016/j.optmat.2015.09.008.

Polymeris, G.S., Goudouri, O.M., Kontonasaki, E., Paraskevopoulos, K.M., Tsirliganis, N. C., Kitis, G., 2011. Thermoluminescence as a probe in bioactivity studies; the case of 58S sol–gel bioactive glass. J. Phys. D. 44, 395501 https://doi.org/10.1088/0022-3727/44/39/395501.

Polymeris, G.S., Giannoulatou, V., Kyriakidou, A., Sfampa, I.K., Theodorou, G.S., Şahiner, E., Paraskevopoulos, K.M., 2017. Bioactivity characterization of 45S5 bioglass using TL, OSL and EPR: comparison with the case of 58S sol-gel bioactive glass. Mater. Sci. Eng. C 70, 673–680. https://doi.org/10.1016/j.msec.2016.09.051.

Portakal Ucar, Z.G., Akca, S., Dogan, T., Halefoglu, Y.Z., Kaynar, U.H., Ayvacikli, M., Garcia Guinea, J., Topaksu, M., Can, N., 2020. Comprehensive study of photoluminescence and cathodoluminescence of Eu and Tb doped Mg_2SiO_4 prepared via a solid-state reaction technique. Opt. Mater. 100, 109698 https://doi.org/10.1016/j.optmat.2020.109698, 2020.

Sarikci, S., Topaksu, M., Madkhali, O., Can, N., 2023. Thermoluminescence characteristics and kinetic analyses of europium doped strontium gadolinium oxide phosphor. Appl. Radiat. Isot. 191, 110549 (2023).

Shwetha, M., Eraiah, B., 2018. Influence of europium (Eu^{3+}) ions on the optical properties of lithium zinc phosphate glasses. IOP Conf. Ser. Mater. Sci. Eng. 310, 012033 https://doi.org/10.1088/1757-899X/310/1/012033.

Silva, A.M.B., Junot, D.O., Caldas, L.V.E., Souza, D.N., 2020. Structural, optical and dosimetric characterization of $CaSO_4$:Tb, $CaSO_4$:Tb, Ag and $CaSO_4$:Tb,Ag(NP). J. Lumin. 224, 117286 https://doi.org/10.1016/j.jlumin.2020.117286.

Silva, A.M.B., Silveira, W.S., Matos, T.S., Junot, D.O., Rezende, M.V.S., Souza, D.N., 2021. Effect of terbium and silver co-doping on the enhancement of photoluminescence in $CaSO_4$ phosphors. Opt. Mater. 111, 110717 https://doi.org/10.1016/j.optmat.2020.110717.

Silva, A.M.B., Souza, L.F., Antonio, P.L., Junot, D.O., Caldas, L.V.E., Souza, D.N., 2022. Effects of manganese and terbium on the dosimetric properties of $CaSO_4$. Radiat. Phys. Chem. 198, 110207 https://doi.org/10.1016/j.radphyschem.2022.110207.

Tamrakar, R.K., Tiwari, N., Kuraria, R.K., Bisen, D.P., Dubey, V., Upadhyay, K., 2015. Effect of annealing temperature on thermoluminescence glow curve for UV and gamma ray induced ZrO_2: Ti phosphor. J. Radiat. Res. Appl. Sci. 8, 1–10. https://doi.org/10.1016/j.jrras.2014.10.005.

Tekin, H.O., Al-Buriahi, M.S., Issa, S.A., Zakaly, Hesham M.H., Issa, Bashar, Kebaili, I., Badawi, A., Karim, M.K.A., Matori, K.A., Zaid, M.H.M., 2021. Effect of Ag_2O substituted in bioactive glasses: a synergistic relationship between antibacterial zone and radiation attenuation properties. J. Mater. Res. Technol. 13, 2194–2201. https://doi.org/10.1016/j.jmrt.2021.06.025.

Valença, J.V.B., Silva, A.C.A., Dantas, N.O., Caldas, L.V.E., d'Errico, F., Souza, S.O., 2018. Optically stimulated luminescence of the 20Li2CO3 – (X)K2CO3 – (80 - X) B2O3 glass system. J. Lumin. 200, 248–253. https://doi.org/10.1016/j.jlumin.2018.03.060.

Yang, B., Yang, Z., Liu, Y., Lu, F., Li, P., Yang, Y., Li, X., 2012. Synthesis and photoluminescence properties of the high-brightness Eu^{3+}-doped $Sr_3Y(PO_4)_3$ red phosphors. Ceram. Int. 38, 4895–4900. https://doi.org/10.1016/j.ceramint.2012.02.080.

Yukihara, E.G., Milliken, E.D., Doull, B.A., 2014. Thermally stimulated and recombination processes in MgB_4O_7 investigated by systematic lanthanide doping. J. Lumin. 154, 251–259. https://doi.org/10.1016/j.jlumin.2014.04.038.

Ziya Halefoglu, Yusuf, Oglakci, M., Yuksel, M., Canimoglu, A., Topaksu, M., Can, N., 2019. Structural and spectroscopic properties of $LaAlBO_3$ doped with Eu^{3+} ions. Appl. Radiat. Isot. 154, 969–8043. https://doi.org/10.1016/j.apradiso.2019.108876.